

Supplementary Materials for

Electrodeposited surfaces with reversibly switching interfacial properties

Yue Liu, Liyan Zhao, Jianjian Lin, Shikuan Yang*

*Corresponding author. Email: shkyang@zju.edu.cn

Published 1 November 2019, *Sci. Adv.* **5**, eaax0380 (2019)

DOI: 10.1126/sciadv.aax0380

The PDF file includes:

- Fig. S1. Characterization of the silver porous membrane.
- Fig. S2. Roughness characterization of the electrodeposited silver porous membranes.
- Fig. S3. An optical image of an oil droplet (here, lubricant Krytox 102 obtained from DuPont, USA) spreading on the as-prepared silver porous membrane.
- Fig. S4. Sensing of ethanol.
- Fig. S5. Cyclic voltammetry measurement.
- Fig. S6. XPS characterization.
- Fig. S7. SERS mapping results.
- Fig. S8. No wettability switch was observed on the electrodeposited pure silver nanoparticle film.
- Fig. S9. Design rationale of the electrodeposited membranes with reversibly switching interfacial properties.
- Fig. S10. The effect of the alkyl chain length on the wettability transition performance.
- Fig. S11. Compatibility of the electrodeposition method to the sophisticated micro/nanofabrication techniques.
- Fig. S12. Schematic illustration of the setup used in information encryption application.
- Fig. S13. Creating superhydrophobic tracks on a superhydrophilic silver porous membrane.
- Fig. S14. Droplet transfer.
- Fig. S15. Water harvesting performance on different surfaces.

Other Supplementary Material for this manuscript includes the following:

(available at advances.sciencemag.org/cgi/content/full/5/11/eaax0380/DC1)

Movie S1 (.mov format). The superhydrophilicity of the as-electrodeposited silver porous membrane.

Movie S2 (.mov format). The superhydrophobicity of the organic reagent-treated silver porous membrane.

Movie S3 (.mov format). The repellency of oil droplets of SLIPS 1.
Movie S4 (.mov format). The repellency of water droplets of SLIPS 2.

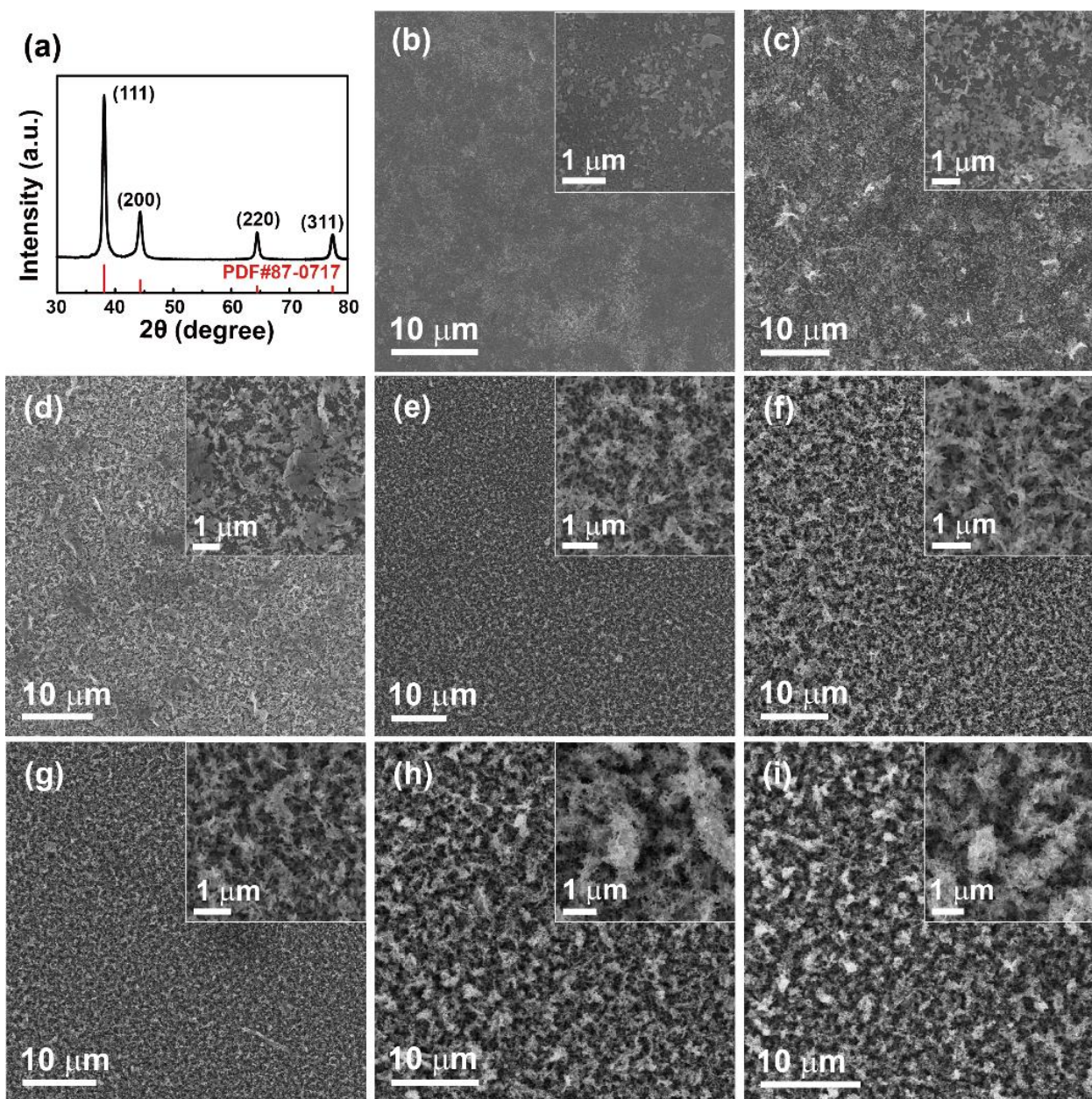


Fig. S1. Characterization of the silver porous membrane. a, The X-ray diffraction pattern of the electrodeposited membranes. b to i, Scanning electron microscope images of the silver porous membranes electrodeposited at 1.5 V for 0.5 min, 1 min, 2 min, 3 min, 4 min, 6 min, 8 min, and 10 min, respectively. Inset: the enlarged image.

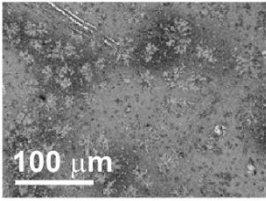
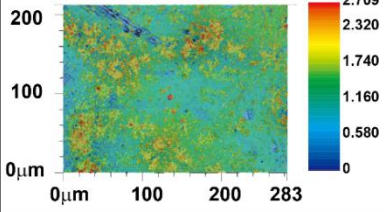
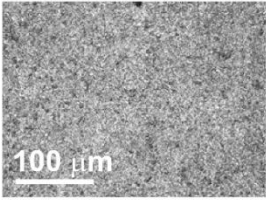
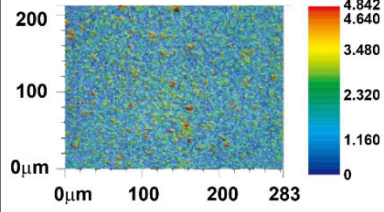
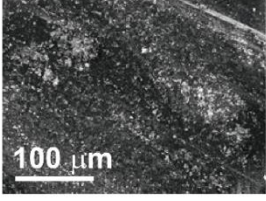
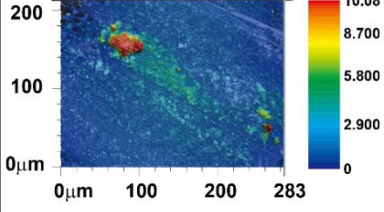
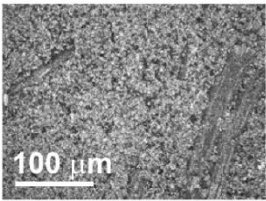
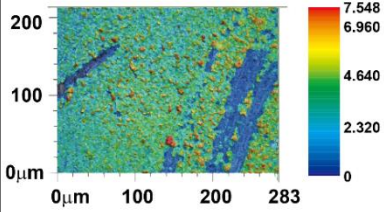
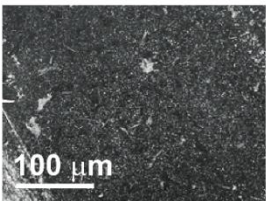
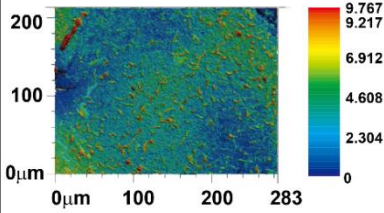
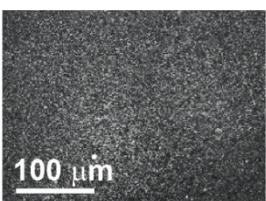
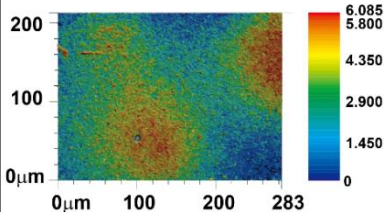
SEM images	Optical images	Arithmetic mean height
		0.070
		0.209
		0.327
		0.368
		0.404
		0.416

Fig. S2. Roughness characterization of the electrodeposited silver porous membranes. a to f, the scanning electron microscope images, the microscopic topography images, and the corresponding values (μm) of the arithmetic average height for the porous membranes electrodeposited at 1.5 V for 0.5 min, 1 min, 2 min, 4 min, 8 min, and 10 min, respectively. The color in the microscopic topography images reflected the heights.



Fig. S3. An optical image of an oil droplet (here, lubricant Krytox 102 obtained from DuPont, USA) spreading on the as-prepared silver porous membrane.

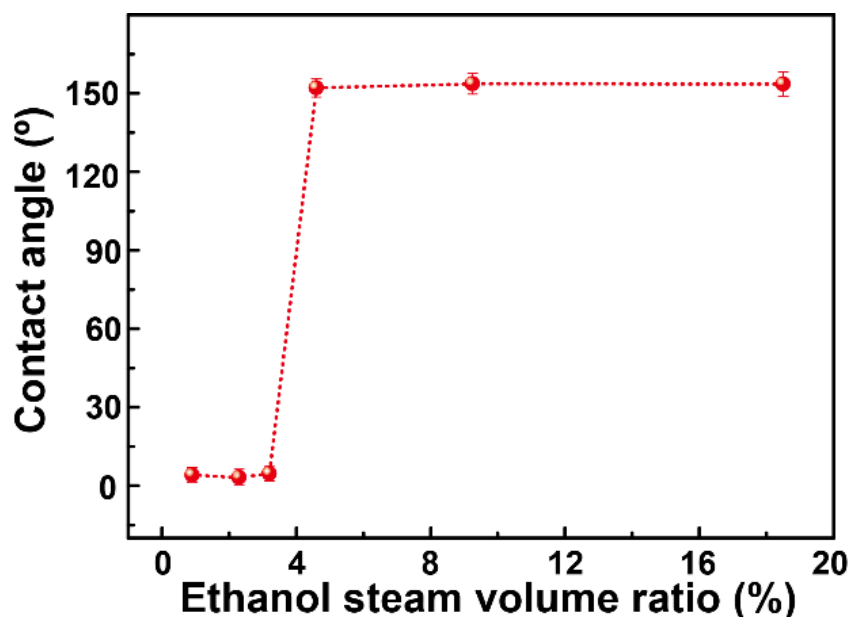


Fig. S4. Sensing of ethanol. The water contact angle of the porous membrane after being exposed to the ethanol environment for three minutes. The ethanol environment was created by evaporating a certain volume of ethanol in a sealed container. The volume of the liquid ethanol over that of the chamber was deemed as the ethanol steam volume ratio. Six ratios, *i.e.*, 0.9 %, 2.3 %, 3.2 %, 4.6 %, 9.25 %, and 18.5 %, were studied. The error bars were obtained based on three independent measurements.

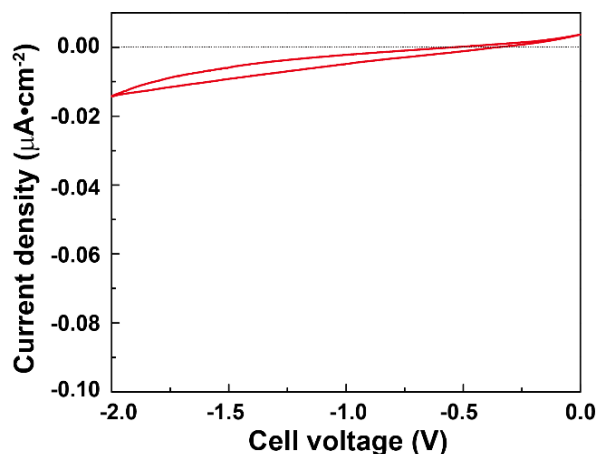


Fig. S5. Cyclic voltammetry measurement. Cyclic voltammetry was used to study the redox reactions during the wettability switch of the silver porous membrane under an electrical potential. The cyclic voltammetry was measured by immersing the silver porous membrane into water composed of 0.5 mM boric acid. The scan rate of the voltage was 0.05 V/s. No obvious redox reactions were observed during the wettability switch process.

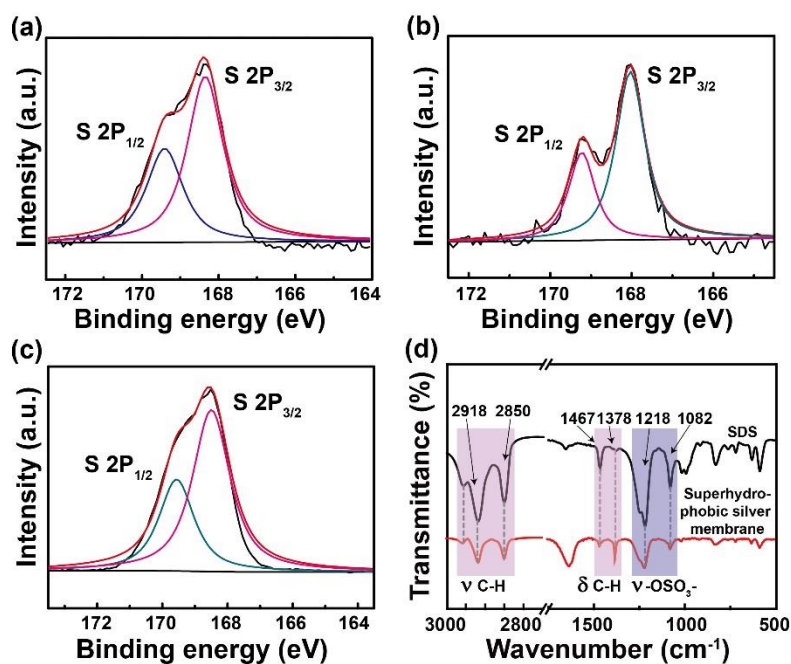


Fig. S6. XPS characterization. **a** to **c**, The binding energy of sulfur element in the superhydrophilic and the superhydrophobic porous silver membrane, as well as the pure sodium dodecyl sulfate powder, respectively. **d**, FTIR spectrum of pure sodium dodecyl sulfate (SDS) powder and the as-prepared silver porous membrane. The absorption peaks at 2918 cm^{-1} and 2850 cm^{-1} are originated from the stretching mode (ν) of C-H. The 1467 cm^{-1} and 1378 cm^{-1} are arising from the bending mode (δ) of C-H. The stretching mode of the $-\text{OSO}_3^-$ leads to the appearance of the 1218 cm^{-1} and 1082 cm^{-1} absorption peaks.

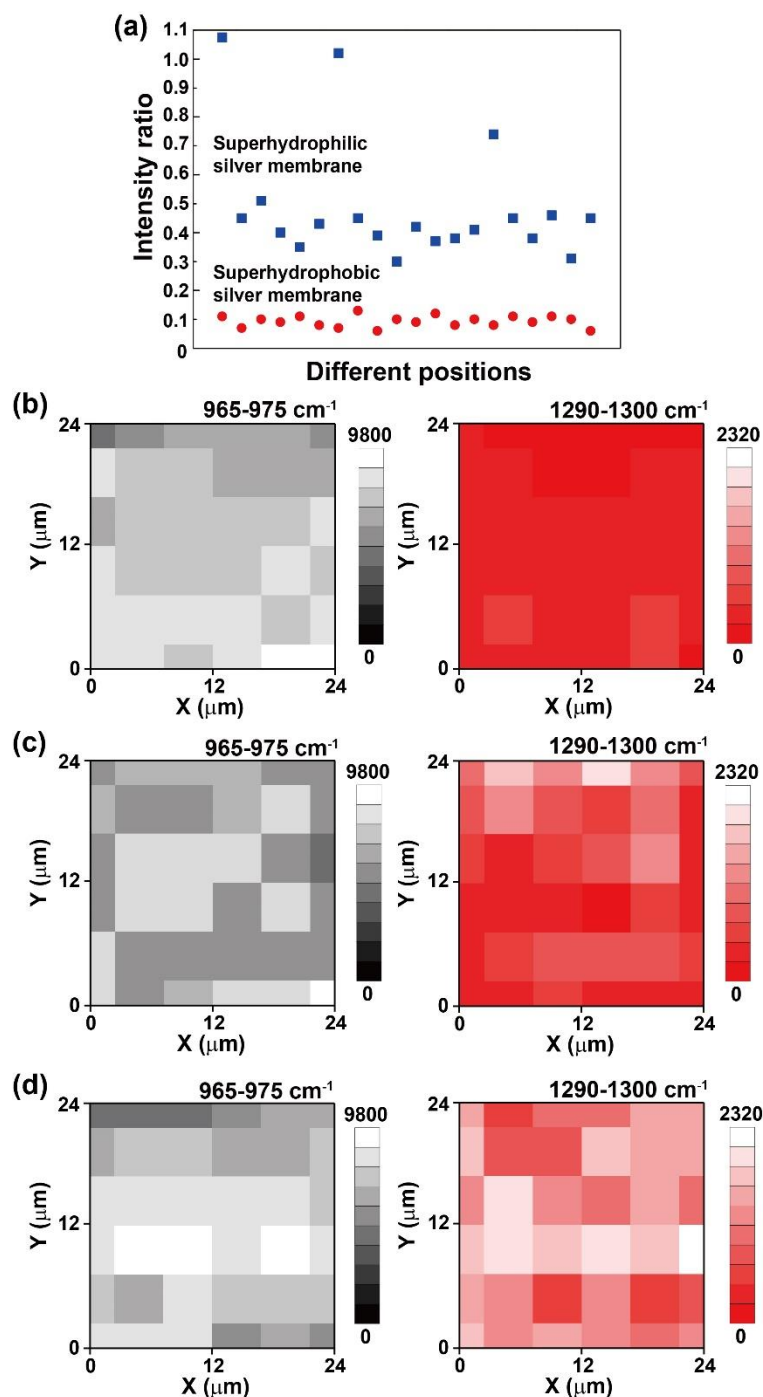


Fig. S7. SERS mapping results. **a**, The intensity ratio between the 963 cm^{-1} SERS peak (from silver sulfate) and the 1297 cm^{-1} SERS peak (from dodecyl chains) at superhydrophilic state and superhydrophobic state at random positions of the silver porous membrane. **b** to **d**, The SERS mapping results of the vibration mode of silver sulfate and dodecyl sulfate chains when the superhydrophobic membrane was under 2 V treatment for 5 min, 10 min, and 15 min, respectively.

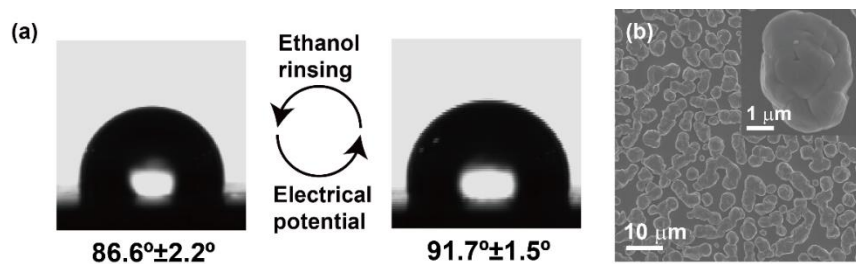


Fig. S8. No wettability switch was observed on the electrodeposited pure silver nanoparticle film. **a**, The water contact angle was $86.6^\circ \pm 2.2^\circ$ for the as-deposited pure silver nanoparticle film. After ethanol rinsing, the contact angle was only slightly changed to $91.7^\circ \pm 1.5^\circ$. **b**, Scanning electron microscope image of the electrodeposited pure silver nanoparticle film. Inset: enlarged observation.

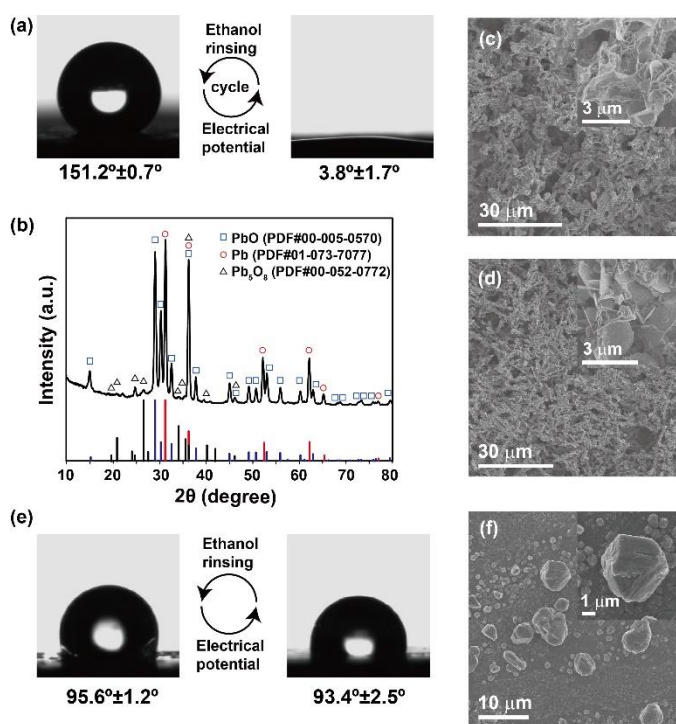


Fig. S9. Design rationale of the electrodeposited membranes with reversibly switching interfacial properties. **a**, The wettability of the lead/lead oxide membrane could be reversibly switched from superhydrophilic to superhydrophobic. **b**, X-ray diffraction pattern of the electrodeposited lead/lead oxide membrane. **c** and **d**, The scanning electron microscope image of the membrane at superhydrophobic and superhydrophilic state, respectively. The morphology was not changed after the wettability switch for multiple times. **e**, The water contact angle was maintained at around 95° on the electrodeposited copper nanoparticle film after ethanol rinsing or being subject to an electrical potential. No wettability switch was observed on electrodeposited copper nanoparticle films. **f**, The scanning electron microscope image of the electrodeposited copper nanoparticle film.

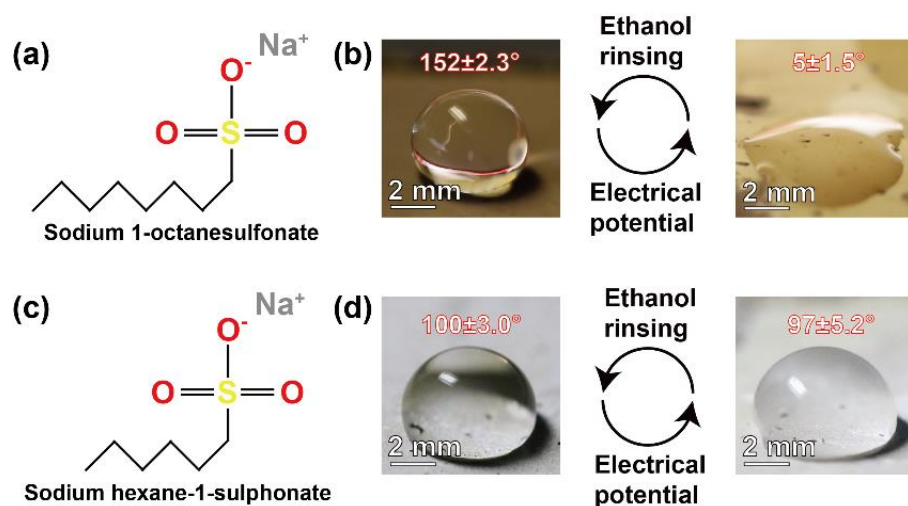


Fig. S10. The effect of the alkyl chain length on the wettability transition performance. **a**, The silver porous membrane could be reversibly switched from superhydrophobic to superhydrophilic when sodium 1-octanesulfonate was used. **b**, No wettability transition was observed on the silver porous membrane prepared using sodium hexane-1-sulphonate. (Photo Credit: Yue Liu, Zhejiang University)

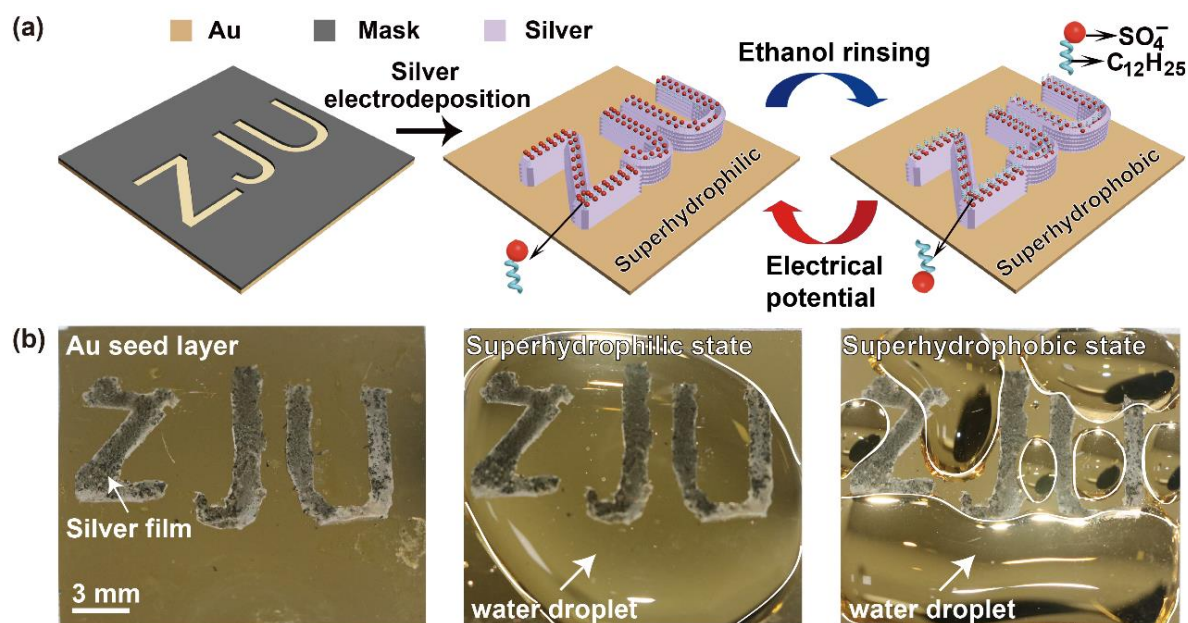


Fig. S11. Compatibility of the electrodeposition method to the sophisticated micro/nanofabrication techniques. **a**, Schematic illustration of fabricating patterned porous silver membranes through electrodeposition on the gold film protected by a “ZJU” shaped mask. **b**, Digital photographs showing the reversibly switching wettability of the patterned silver porous membranes. The as-prepared “ZJU” letters were superhydrophilic. After ethanol rinsing, the “ZJU” letters turned to superhydrophobic. The superhydrophobic “ZJU” letters turned back to superhydrophilic after being subject to an electrical potential. (Photo Credit: Yue Liu, Zhejiang University)

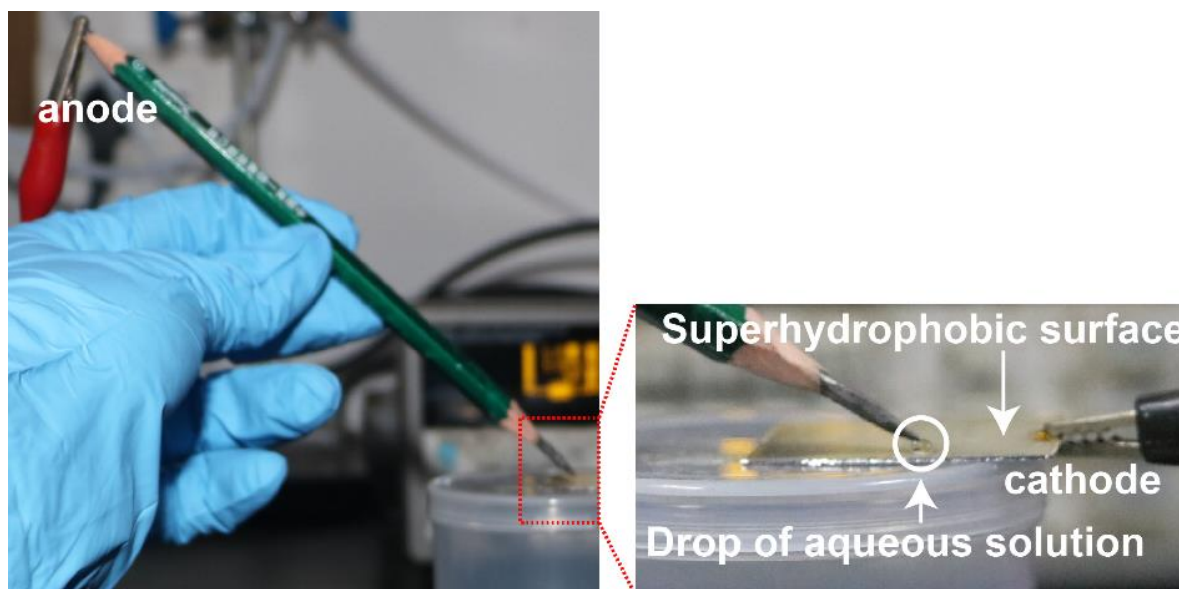


Fig. S12. Schematic illustration of the setup used in information encryption application. (Photo Credit: Yue Liu, Zhejiang University)

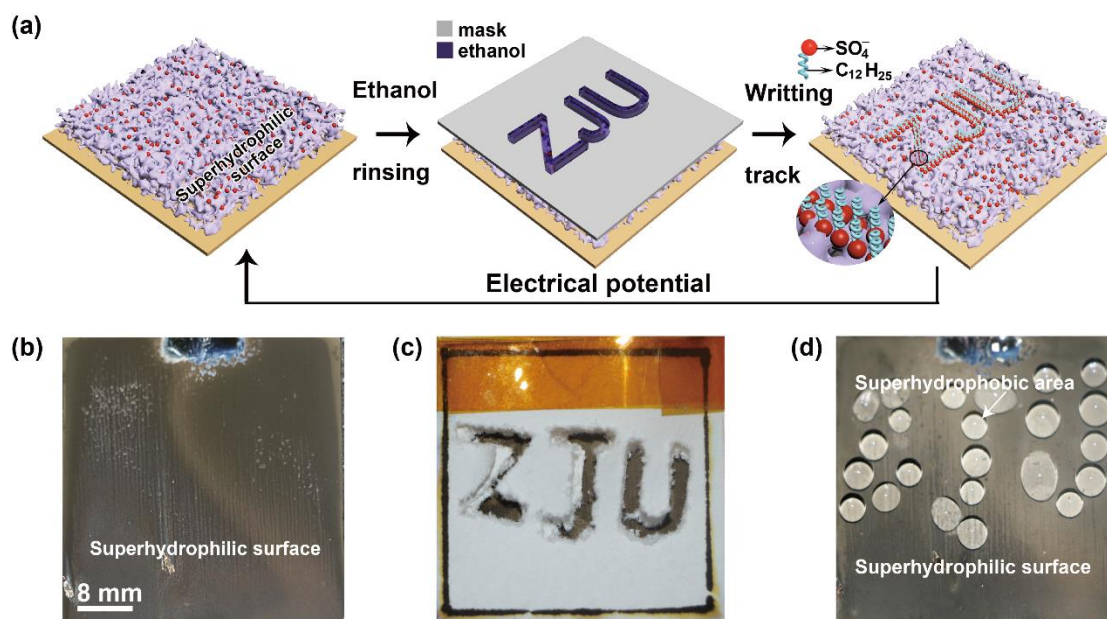


Fig. S13. Creating superhydrophobic tracks on a superhydrophilic silver porous membrane. **a**, Schematic of creating superhydrophobic “ZJU” letters on the superhydrophilic porous membrane. Ethanol was sprayed onto the superhydrophilic porous membrane covered with a mask with “ZJU” letters. The “ZJU” letters were changed into superhydrophobic. The superhydrophobic “ZJU” letters turned to superhydrophilic after being subject to an electrical potential. **b**, The optical image of the superhydrophilic porous membrane. **c**, Ethanol was applied onto the mask on the superhydrophilic porous membrane. **d**, The “ZJU” letters turned to superhydrophobic. (Photo Credit: Yue Liu, Zhejiang University)

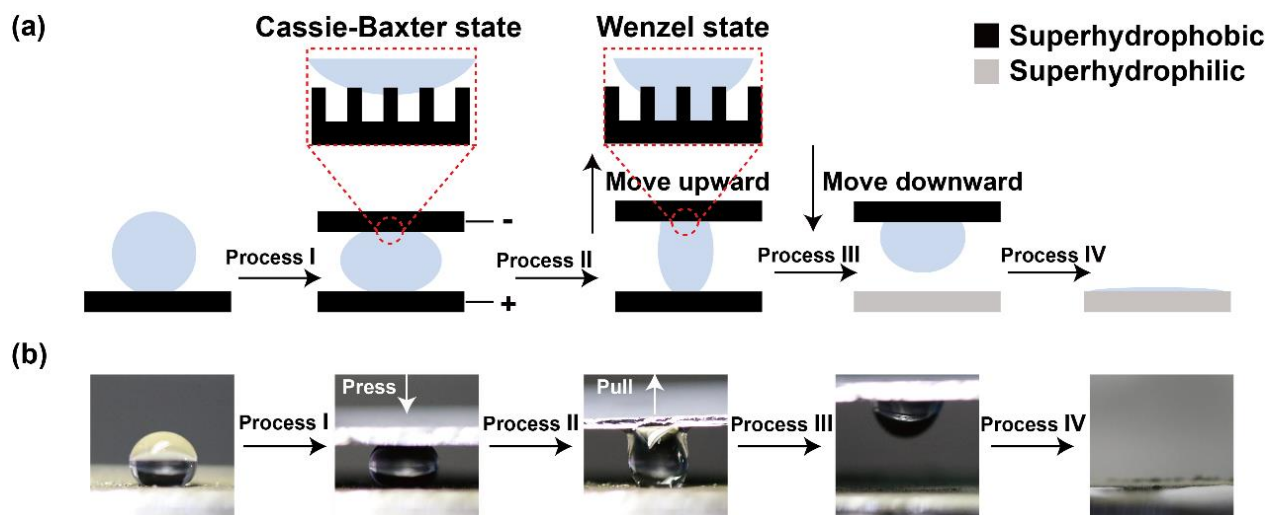


Fig. S14. Droplet transfer. **a**, The process of water droplet transportation using silver porous membranes. Process I: The water droplet was sandwiched between two superhydrophobic surfaces at a Cassie-Baxter state, with the top one connected to the negative pole and the bottom one connected to the positive pole of a power supply. Process II: The interface between the droplet and the top porous membrane would turn to hydrophilic at a Wenzel state. The hydrophilic area had a strong adhesion force to the water droplet. Therefore, when the top porous membrane was lifted up, the water droplet was transferred onto the top porous membrane from the bottom porous membrane. Process III: The droplet would be transferred onto another surface when the porous membrane was moving close to it. **b**, Experimental demonstration of the droplet transfer process. (Photo Credit: Yue Liu, Zhejiang University)

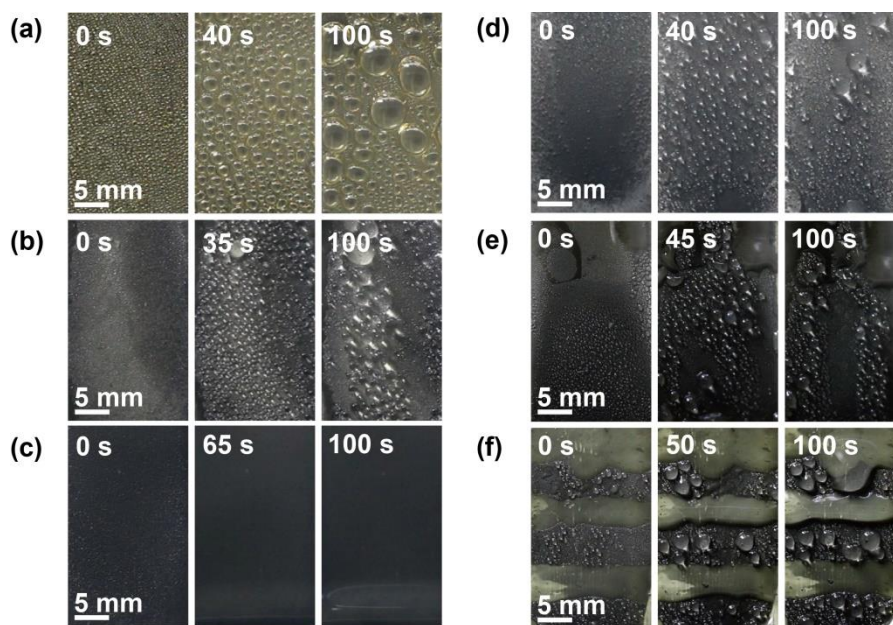


Fig. S15. Water harvesting performance on different surfaces. a to f, The photographs of water droplets at different time intervals on the gold film, the superhydrophobic porous membrane, the superhydrophilic porous membrane, SLIPS 2, the surface composed of superhydrophilic porous membrane at the top half area and SLIPS 2 at the bottom half area, and the surface composed of alternately arranged superhydrophilic surface and SLIPS 2, respectively. SLIPS 2 was formed by infusing lubricant Krytox 102 inside the porous membrane. (Photo Credit: Yue Liu, Zhejiang University)